Earthquake Source Complexity Controls the Frequency-Dependence of Near-Source Radiation Patterns

Daniel T. Trugman[1], Shanna X Chu[2], and Victor Chen Tsai[2]

[1]The University of Texas at Austin
[2]Brown University

November 24, 2022

Abstract

The spatial patterns of earthquake ground motion amplitudes are commonly represented using a double couple model that corresponds to shear slip on a planar fault. While this framework has proven successful in explaining low-frequency seismic recordings, at higher frequencies the wavefield becomes more azimuthally isotropic for reasons that are not yet well understood. Here we use a dense array of nodal seismometers in Oklahoma to study the radiation patterns of earthquakes in the near-source region where wavefield scattering effects are limited. At these close distances, the radiation pattern is predominantly double couple at low frequencies (<15Hz). At higher frequencies, the recorded wavefield contains significant isotropic and residual components that cannot be explained as path or site effects, implying complexity in the rupture process or local fault zone structure. These findings demonstrate that earthquake source complexity can drive variability in the ground motions that control seismic hazard.

Hosted file

`radpattern-lasso_esupp-v06-grl.docx` available at https://authorea.com/users/549063/articles/604628-earthquake-source-complexity-controls-the-frequency-dependence-of-near-source-radiation-patterns

Hosted file

`essoar.10507460.1.docx` available at https://authorea.com/users/549063/articles/604628-earthquake-source-complexity-controls-the-frequency-dependence-of-near-source-radiation-patterns

Daniel T. Trugman[1], Shanna X. Chu[2], Victor C. Tsai[2]

[1] Jackson School of Geosciences, The University of Texas at Austin

[2] Department of Earth, Environmental and Planetary Sciences, Brown University

Corresponding author: Daniel Trugman (`dtrugman@jsg.utexas.edu`)

Key Points:

- We study the frequency-dependence of earthquake radiation patterns in the near-source region using a dense seismometer array.

- At low frequencies (< 15 Hz), radiation patterns show excellent agreement with the double couple model.

- At high frequencies, the double couple radiation pattern deteriorates, likely due to source and fault zone complexity.

Abstract

The spatial patterns of earthquake ground motion amplitudes are commonly represented using a double couple model that corresponds to shear slip on a planar fault. While this framework has proven successful in explaining low-frequency seismic recordings, at higher frequencies the wavefield becomes more azimuthally isotropic for reasons that are not yet well understood. Here we use a dense array of nodal seismometers in Oklahoma to study the radiation patterns of earthquakes in the near-source region where wavefield scattering effects are limited. At these close distances, the radiation pattern is predominantly double couple at low frequencies (<15Hz). At higher frequencies, the recorded wavefield contains significant isotropic and residual components that cannot be explained as path or site effects, implying complexity in the rupture process or local fault zone structure. These findings demonstrate that earthquake source complexity can drive variability in the ground motions that control seismic hazard.

Plain Language Summary

The amplitude of the ground motions produced by an earthquake is not constant in all directions, but instead varies systematically in relation to the orientation of the fault on which the earthquake occurs. Here we study these directional variations in ground motions, known as the seismic radiation pattern, using a large dataset of thousands of closely spaced seismometers recording nearby earthquakes. Our focus is on understanding how the spatial pattern of ground motions depend on their frequency of the vibration. We find that at low frequencies, a simplified and widely-used four-lobed model of earthquake ground motions does a good job describing the observed seismic wavefield. At higher frequencies, however, this four-lobed radiation pattern begins to deteriorate due to complexity in the earthquake source and fault zone structure. Understanding the physical mechanisms driving spatial variations in ground motion will help

1

create more accurate earthquake hazard forecasts for communities living near active faults.

1 Introduction

In many ways, the progression of our understanding of the seismic radiation pattern of earthquakes has mirrored the evolution of earthquake science itself. By the early 1900s (Reid, 1911), it was well understood that earthquakes represented shear slip on faults at depth within the Earth's crust. However, connecting this heuristic understanding with more sophisticated theoretical models of the earthquake source proved surprisingly difficult. In the 1920s, Nakano (Nakano, 1923) suggested that the recorded ground motions from earthquakes may be explained in terms of a double couple representation of the earthquake source. This hypothesis remained controversial for nearly forty years, until a series of theoretical and observational studies (Balakina et al., 1961; Burridge & Knopoff, 1964; Honda, 1962; Vvedenskaya, 1956), combined with routine estimation of earthquake mechanisms made possible through the advent of the World-Wide Network of Seismograph Stations (Oliver & Murphy, 1971) definitively demonstrated the double couple model's validity. To this day, knowledge of the radiation pattern of a double couple source is fundamental to many problems in seismology and is thus a cornerstone of many introductory classes in earthquake science.

While it is widely acknowledged that real earthquake sources may deviate from a theoretical double couple in important ways (Frohlich, 1994; Hayashida et al., 2020; Julian et al., 1998), the double couple model has proven remarkably successful in explaining the radiation pattern of earthquakes at long periods (frequencies less than ~ 2 Hz). At higher frequencies, however, the situation becomes more complicated and the model notably less satisfactory (Castro et al., 2006). The effects of scattering become more pronounced at higher frequencies and longer source-receiver recording distances (Aki & Chouet, 1975), an effect which serves to homogenize the wavefield relative to the double couple prediction (Kobayashi et al., 2015; Takemura et al., 2009, 2016). In addition, the mixture and coupling of SV and SH waves can generate additional frequency-dependent distortion of the radiation pattern (Satoh, 2002; Takenaka et al., 2003). While these two mechanisms are essentially path effects, complexity in the earthquake source may also drive frequency-dependent distortions in the radiation pattern (Liu & Helmberger, 1985), for example through heterogeneity in the rupture process (Graves & Pitarka, 2016), fault zone complexity (Chester & Chester, 1998; Faulkner et al., 2003), or fault roughness (Fang & Dunham, 2013; Trugman & Dunham, 2014). Understanding this distinction between source and path effects is not just of scientific interest but also of practical importance, as quantitative constraints on the spatial distribution of high-frequency ground motions is fundamental to earthquake hazard analysis.

Here we seek to unravel this issue through densely recorded, near-source observations of small earthquakes in Oklahoma. We use measurements of the P-wave radiation patterns of local earthquakes captured by the LArge-N Seismic

2

Survey (LASSO), an 1829-station temporary deployment in an area of induced seismicity in northern Oklahoma (Dougherty et al., 2019), to quantify frequency-dependent deviations in the recorded wavefield from the theoretical double couple prediction. Because of its dense station coverage in the near-source region, the cumulative path effects of scattering are less severe and source effects are more readily observed. We focus our attention on a subset of well-recorded, strike-slip events with clear double couple radiation patterns at low frequencies. For each event, we decompose the recorded wavefield into double couple, isotropic and residual terms, and explore the frequency dependence of each. In doing so, we aim to leverage the unique advantages of the LASSO dataset in order to provide new insights into the physical mechanisms underlying the frequency-dependent distortion of radiation pattern.

2 Dataset and Methodology

The LASSO array was a 2016 USGS-led field deployment of vertical-component nodal seismometers in Grant County, an area of northern Oklahoma subject to sustained hydrocarbon development. During the experiment, an array of 1833 Fairfield Nodal ZLand 1C seismometers with 500Hz sampling rate were deployed over an area of 25 km by 32 km, with typical station spacing of 400 m. A total of 1829 of these seismometers maintained full operation during the 28-day deployment in April and May of 2016. The array recorded an active area of seismicity throughout its deployment, and several recent studies have highlighted various features of these earthquakes, including remote dynamic triggering effects (Peña Castro et al., 2019), spatiotemporal clustering of seismicity (Cochran et al., 2020), and source spectral properties (Kemna et al., 2020). Our work builds upon these early findings, in particular using the event catalog of Cochran et al. (2020) as a starting point for our analysis. For these events, we download publicly available waveform data from IRIS (network code 2A) and develop an automated procedure to extract P-wave arrivals and first motions (Text S1 and Figure S1 in the electronic supplement).
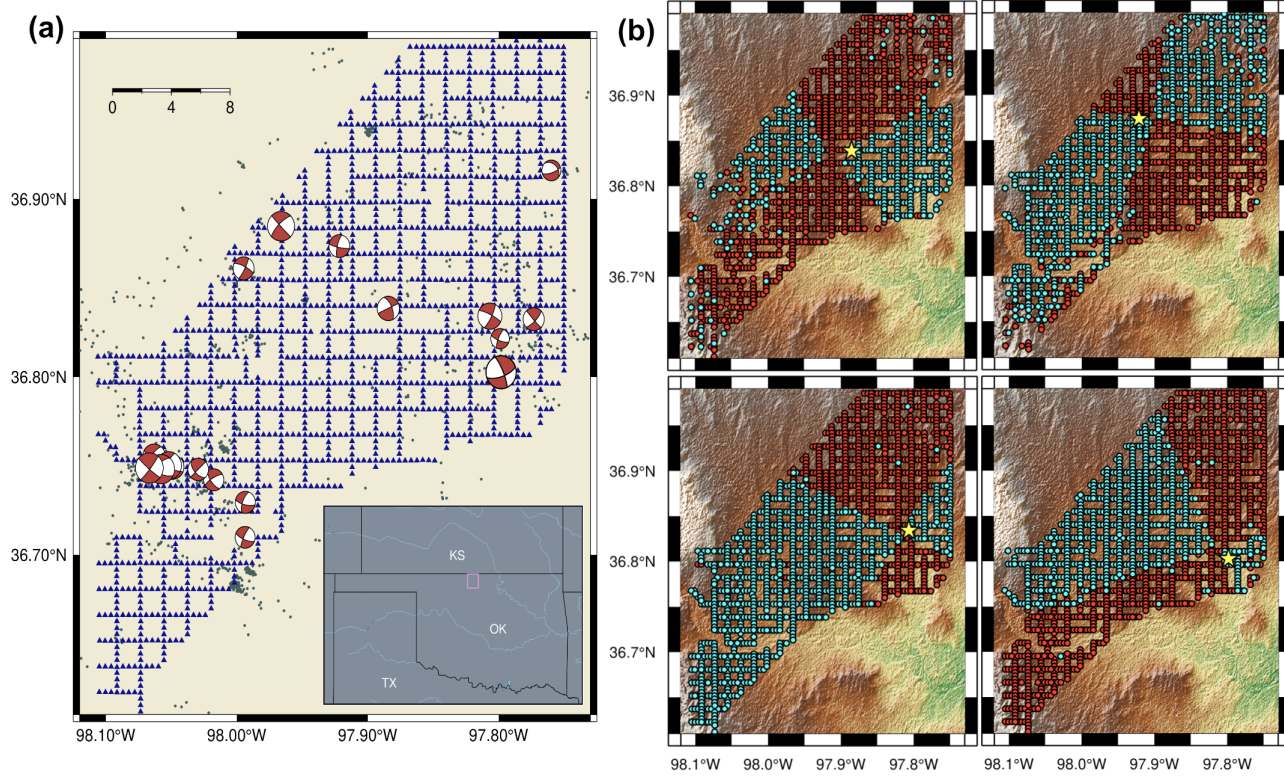
Figure 1. Study region and first motion polarities. (a) Locations and focal mechanisms for the subset of twenty-four analyzed events. (b) Examples of first motion estimates for four different earthquakes (marked with stars) in our dataset. Positive and negative polarities are colored in red and blue respectively.

Our analysis centers on a subset of 24 earthquakes occurring within the footprint of the LASSO array and that have good azimuthal station coverage (Fig. 1a, Table S1). These events range in size from local magnitude M_L 1.70 to 2.76 and have predominantly strike-slip mechanisms with clear azimuthal variations in P-wave first motion polarities across the array (Fig. 1b). Our main objective is to measure if there are frequency-dependent deviations in the observed radiation pattern of earthquakes from that of a pure double couple. To accomplish this, for each event we bandpass filter the waveforms recorded at each station into eight different frequency bands up to 35 Hz and spanning the dominant spectrum of interest (Text S2). We then measure the root-mean-square (RMS) amplitude of the direct P-wave within a 0.2 s time window immediately following the phase arrival. While the overall results are rather insensitive to the time window length (Figure S2), the 0.2-s duration was selected to fully capture the direct P-wave pulse of each event while still being short enough to avoid potential bias from the inclusion of scattered phases or background noise. We correct the observed RMS amplitudes for distance-dependent and event offset effects using

4

a regression analysis that includes both geometric spreading and attenuation terms (Text S3, Figure S3). This effectively normalizes the data to facilitate direct comparison with theoretical models of the radiation pattern.

To isolate different physical contributions to the observed spatial patterns of ground motion, we decompose the normalized wavefield $\widetilde{\mathbf{A}}_{\mathrm{obs}}$ in each frequency band into the sum of a double couple term $\mathbf{A}_{\mathrm{DC}}$, which varies in strength based on the station location (and its azimuth and takeoff angle), and an isotropic term A_{ISO} which is constant at all stations (i.e., equal average radiation in all directions):

$$\widetilde{\mathbf{A}}_{\mathrm{obs}}\,(\,,\,) = \mathrm{p}\; A_{\mathrm{DC}}\,(\,,\,) + (\mathbf{1}-\mathbf{p})\; A_{\mathrm{ISO}} + \;.\; (1)$$

In this formulation, the parameter p represents the strength of a double couple term relative to the isotropic term, with values approaching one indicating strongly double couple and values approaching zero indicating strongly isotropic. The parameter   is a residual term that varies from station to station and represents the misfit between the data and a model consisting of the superposition of double couple and isotropic terms. For each event, we obtain the best-fitting double couple prediction $\mathbf{A}_{\mathrm{DC}}$ by using the first-motion solution (Text S2) as a starting point and optimizing the fit to the data through a grid search procedure performed within the lowest frequency band. Note that by focusing on an RMS measurement, our analysis measures the average energy radiated and does not distinguish between polarities or phases within the 0.2-s window. Because of this, isotropic component of the wavefield A_{ISO} could arise from a wide range of physical processes, not just from a coherent volumetric source.

f-band: 2.50-5.50Hz
double couple pct: 93.9%

f-band: 4.00-8.00Hz
double couple pct: 93.6%

f-band: 6.00-12.00Hz
double couple pct: 92.5%

f-band: 8.00-16.00Hz
double couple pct: 90.0%

f-band: 12.00-20.00Hz
double couple pct: 84.9%

f-band: 16.00-24.00Hz
double couple pct: 72.7%

f-band: 20.00-30.00Hz
double couple pct: 59.2%

f-band: 25.00-35.00Hz
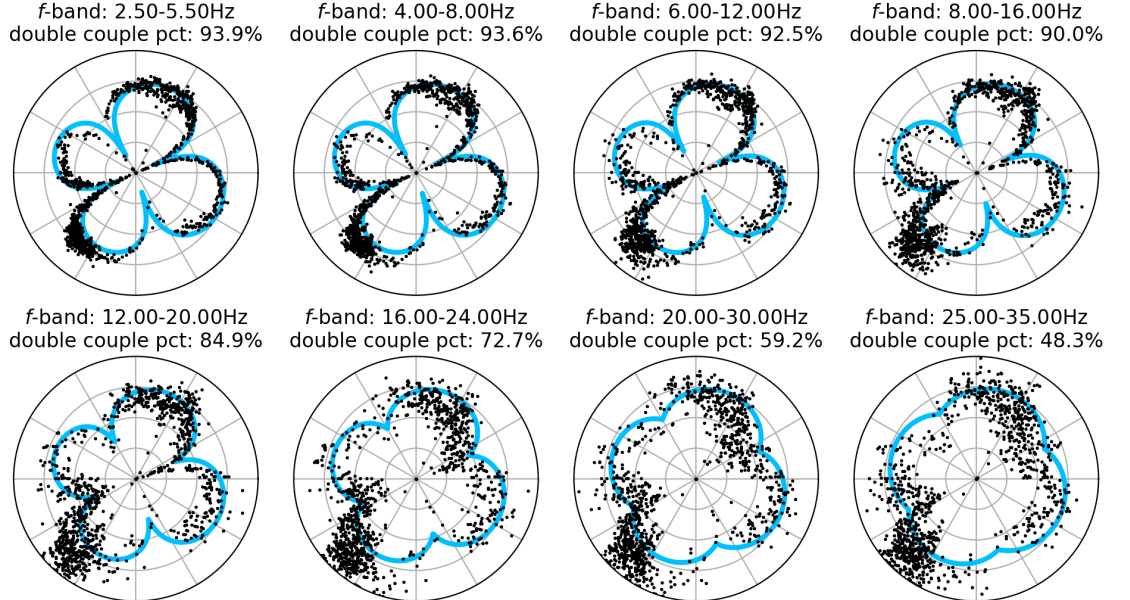double couple pct: 48.3%

Figure 2. Azimuthal distribution of waveform amplitudes in different frequency bands for an example M_L 2.03 earthquake. Measurements are taken from stations with takeoff angles within 20 degrees of horizontal and plotted in black. Model predictions that include both double couple and isotropic components are shown in blue for reference. Each panel corresponds to a different frequency band. The observed radiation pattern becomes increasingly isotropic at higher frequencies and has larger residual scatter.

3 Results

One way to visualize these results is to plot the observed radiation pattern as a function of azimuth within different frequency bands and compare these results to a theoretical prediction. Doing so requires one to select stations within a limited range of raypath takeoff angles (measured from the downward vertical axis at the source), as both the theoretical and observed radiation patterns vary systematically with these takeoff angles. Figure 2 displays the azimuthal dependence of the radiation pattern for a well-recorded M_L 2.03 representative of the others in our dataset. For the events in our dataset, there is typically a strong correlation between the theoretical double couple wavefield at the lowest frequencies we consider ($\sim$ 4 Hz), but the wavefield becomes progressively more isotropic at high frequencies. In our highest frequency band ($\sim$ 30 Hz), for example, the decomposition results suggest that isotropic and residual terms are comparable in strength to the double couple term. It is also illustrative to visualize the full wavefield in map view (Figures 3 and 4) in order to confirm the decomposition results for all stations, regardless of azimuth or takeoff angle. Close inspection of the full wavefield makes it clear that not only the isotropic term but also the relative strength of the residual wavefield increases with increasing frequency. We will discuss this observation and its implication in greater detail in the following section.
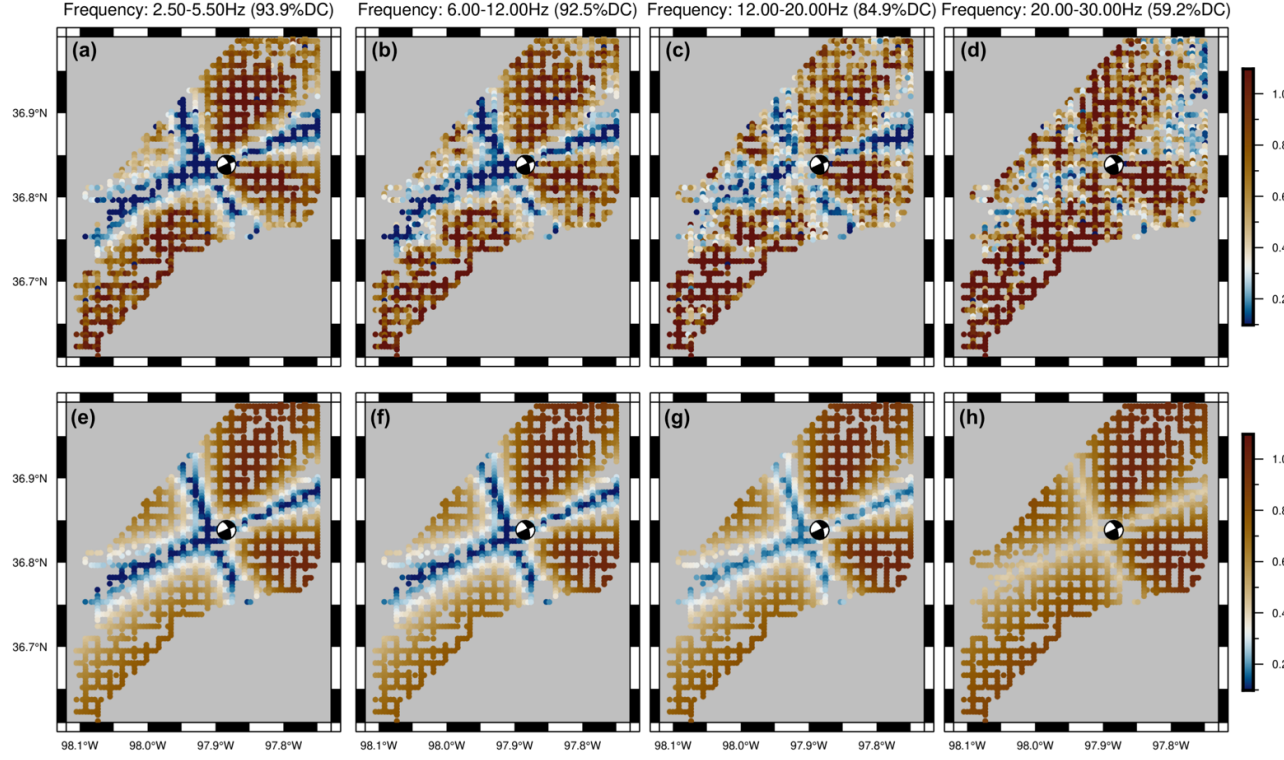
Figure 3. Map view comparisons of the observed radiation pattern (top panels) and model predictions (bottom panels) for the M_L 2.03 earthquake shown in Figure 2. Normalized radiation patterns are displayed with logarithmic colorscale for visual clarity. Panels (a) through (d) show the observations in four increasing frequency bands of the eight total we consider, while panels (e) through (h) show the analogous model predictions.
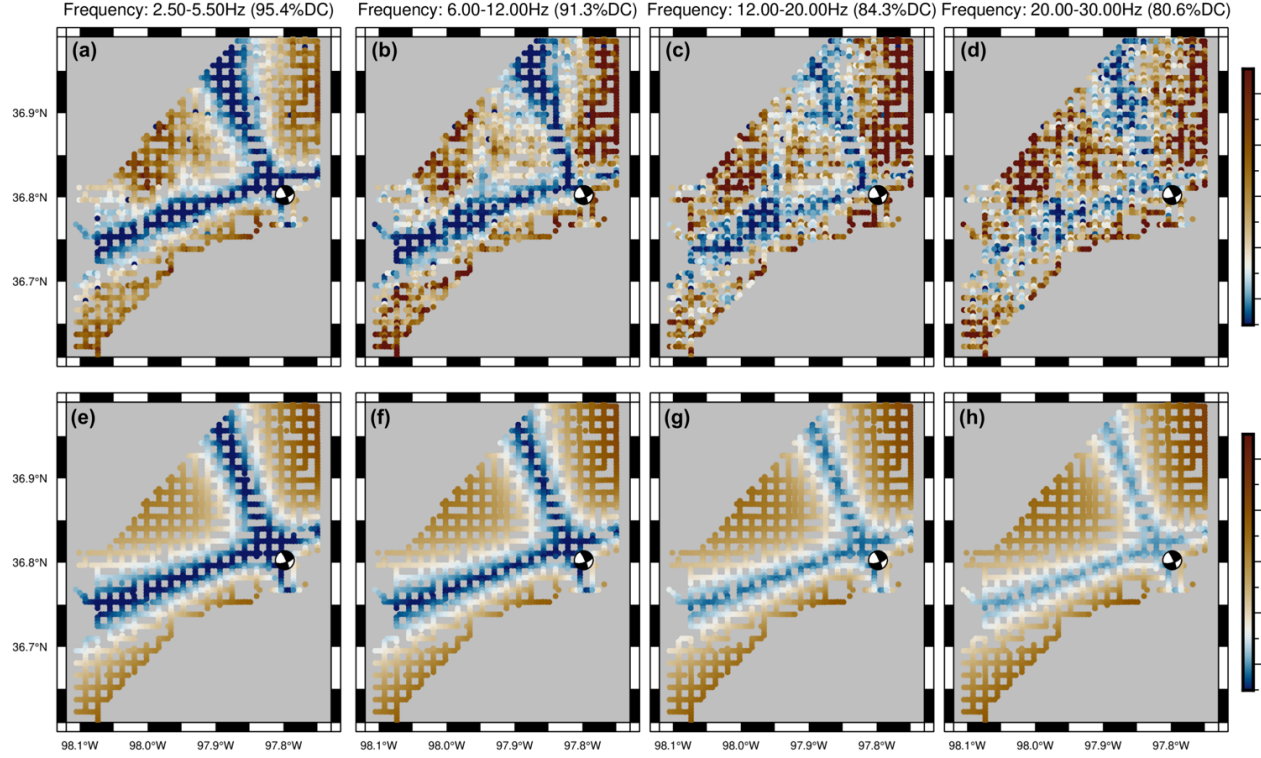
Figure 4. Map view comparisons of the observed radiation pattern model predictions for the largest earthquake in our dataset (M_L 2.76). Panel descriptions are analogous to Figure 3.

We now consider wavefield decomposition results for the full dataset of 24 earthquakes. In Figure 5a, we show boxplots summarizing the statistical distribution of the double couple fraction p in each frequency band. In this figure, we also compare the statistics for the dataset in aggregate to the median values within different magnitude bins. In the lowest frequency bands (< 8 Hz), typical double couple fractions p are of order 0.95 with low variability from event to event and no discernable variability as a function of magnitude. As frequency increases, the double couple fraction consistently declines, with typical values of 0.90 at 10 Hz, 0.78 at 20 Hz and 0.70 at 30 Hz. Variability in the measured double couple fractions also increases markedly with frequency. The larger events in our dataset appear to have slightly higher measured double couple fractions in all frequency bands, though this trend is relatively weak. Indeed, the two largest magnitude bins we consider (M_L 2.1-2.4 and M_L 2.4-2.8) have nearly identical overall statistics.

While our discussion thus far has emphasized the decomposition into double couple and isotropic components, it is also important to consider the residual wavefield that remains unexplained by either of these end-member models. In

Figure 5b, we show the statistical distribution of the median absolute residual within each frequency band. Residual amplitudes are lowest in the lowest frequency bands, with values of order 0.10 typical at ~ 5 Hz. The residuals increase in size with frequency until reaching values of 0.25-0.30 at ~ 30 Hz. The median absolute residual appears to be comparable in size to the isotropic term $(1 - \mathbf{p})$ in each frequency band, though it may be generated by different physical processes. At low frequencies, the double couple term dominates these isotropic and residual terms, but at high frequencies the double couple term is only slightly larger on average.
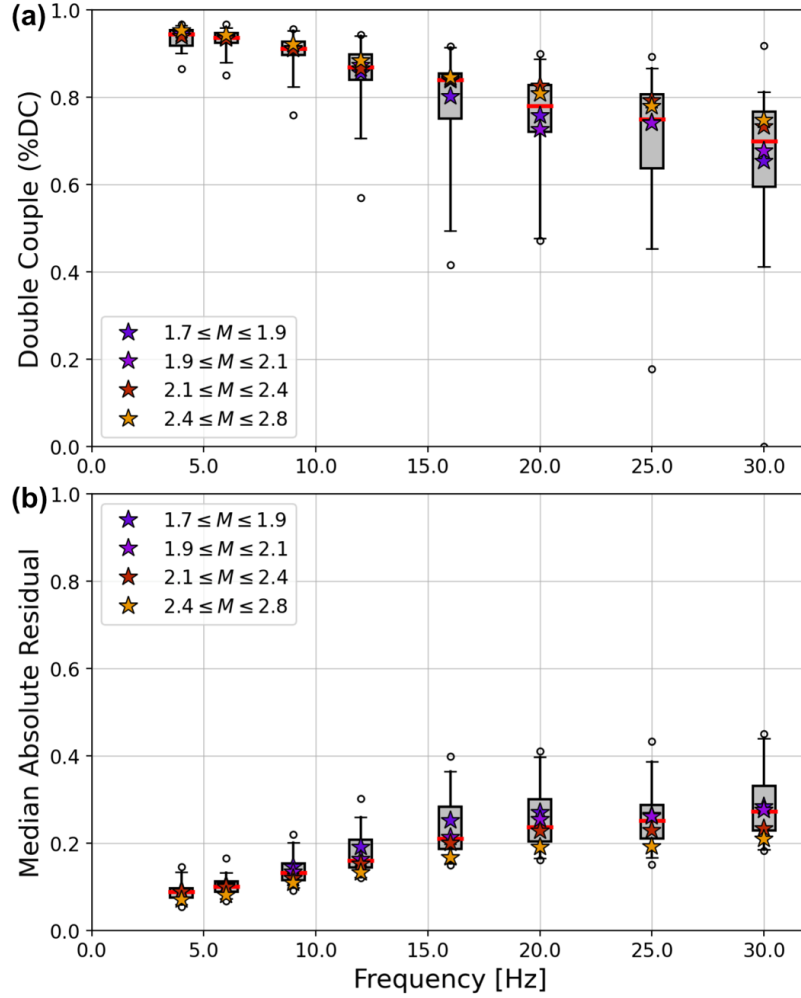
Figure 5. Statistical distributions of frequency-dependent radiation patterns. (a) Boxplot displays of the statistical distribution of double couple fractions (the parameter p in eq. 1) in each frequency band. The red line, box, and whiskers denote the median, interquartile range, and 95% interval respectively. Small

circles denote observations outside this 95% interval. The starred points denote median values in different magnitude bins. (b) Similar to panel (a) but showing the statistical distribution of the median absolute residual between the observed and modeled amplitude.

4 Discussion

In this study, we use observations from the LASSO nodal array in Oklahoma to provide direct, quantitative constraints on the frequency dependence of earthquake radiation patterns. We take advantage of the dense station spacing, good azimuthal coverage, and short source-station distances to push our observations to higher frequencies than in previous work while mitigating the effects of scattering along the raypath. In previous studies focused on the frequency-dependence of the seismic radiation pattern (Castro et al., 2006; Kobayashi et al., 2015; Satoh, 2002; Takemura et al., 2009, 2016; Takenaka et al., 2003), there is broad general agreement that at low frequencies, the observations are well-described by a double couple radiation pattern. A distortion in the radiation pattern at high frequencies may be driven by a number of physical processes, from wavefield scattering to local site effects to source complexity, and unraveling these processes has proven challenging. The LASSO dataset provides a new perspective on this problem through its detailed, near-field measurements collected over a wide frequency range, thus allowing us to isolate the contribution of the earthquake source itself.

The fact that we observe no systematic trends in the residuals or wavefield fits as a function of distance (Figure S4) implies that scattering, which strongly influences the radiation pattern at larger distances (Kobayashi et al., 2015; Takemura et al., 2009), plays a much lesser role in our dataset in which hypocentral distances from source to station range from ~ 3 to 35 km. Though it is possible that scattering could contribute to the measured isotropic or residual terms, if this were the case one would anticipate that the isotropic term would reflect some average level of scattering across the array, and the residual term would vary systematically with distance to compensate for increasing levels of scattering. That we do not see such this trend in our dataset (Figure S4) suggests that other physical mechanisms underly our observations. To further confirm that scattering is not the primary mechanism driving our observations, we tested a model in which the isotropic term increases linearly with distance from the earthquake hypocenter, rather than remain constant across the array. This model, however, did not have lower overall misfit to the data and resulted in an overall ramplike trend with distance in the residuals (Figure S5), implying that the isotropic contribution does not increase with distance as would be expected for a scattering model.

While the favorable geometry of our dataset limits scattering and path attenuation, site effects may remain an important consideration, especially given the rapid deployment and shallow burial depths of LASSO nodal seismometers (Dougherty et al., 2019). One way to quantify the relative importance of site effects is to measure the consistency in the residual terms at each station as col-

lected across different events. If site effects strongly influence the residuals, one would anticipate highly correlated residuals at a given station. Applying this concept to our measurements, we find that site residuals are indeed positively correlated, but at modest levels (0.2 – 0.3, Figure S6) that explain less than 10% of the overall variability in the residual wavefield. Thus, as was the case for scattering, site effects do not appear to be the leading physical mechanism driving the trends in our observations.

Since the observed breakdown in the high-frequency radiation pattern cannot be adequately explained in terms of scattering or site effects, we suggest that complexity in the source process may provide the most viable explanation for our findings. For pure shear slip on a planar fault, the radiation pattern would be fully double couple and independent of frequency. In the LASSO dataset, we observe good agreement with the double couple model at lower frequencies ($<$ 20 Hz) but a growing contribution of isotropic and residual terms as frequencies increase. There are several ways in which such deviations from a purely double couple radiation can arise from source effects, most prominently through higher-order complexity in the rupture process beyond that of shear slip on an idealized planar fault. However, it is important to note that not all forms of rupture complexity will affect the seismic radiation pattern itself. For example, spatial heterogeneity in rise time and rupture velocity may control the overall level of high-frequency seismic radiation, but will not directly influence the radiation pattern of an earthquake on a planar fault (Graves & Pitarka, 2016). In contrast, perturbations to the rake angle or fault orientation along a rough or geometrically complex fault (Dunham et al., 2011; Fang & Dunham, 2013) will distort the radiation pattern at high frequencies while also influencing rupture kinematics (Savran & Olsen, 2020; Trugman & Dunham, 2014). Moreover, many realistic fault zones contain not just a single, isolated and possibly nonplanar fault strand, but rather a system of interacting surfaces and gouge material (Chester & Chester, 1998; Mitchell & Faulkner, 2009; Rowe et al., 2018). The presence of a low-velocity fault zone of finite width can effectively scatter waveform energy during the rupture process (Graves & Pitarka, 2016). Earthquake rupture dynamics is highly sensitive to fault zone complexity (Huang et al., 2014; Huang & Ampuero, 2011; Ma & Elbanna, 2019), which affects the seismic wavefield (Ben-Zion & Ampuero, 2009; Trugman et al., 2020; Tsai & Hirth, 2020).

While our dataset comprises only a limited magnitude range, it is notable that the observed partitioning between double couple, isotropic, and residual terms does not vary strongly with event size. We do observe a modest decrease in residual amplitudes with increasing magnitude (Figure 5b), but this trend can likely be explained as a processing artifact due to better signal-to-noise and more precise waveform onsets for larger earthquakes. For nominal stress drop values in the 1-10 MPa range, we would expect the source spectral corner frequencies for earthquakes in our dataset to range from 6-12 Hz for the largest events to 20-40 Hz for the smallest events. The fact that we do not observe substantial differences between magnitude bins despite their presumably differ-

ent corner frequencies suggests that coherence in the radiation pattern is not controlled by corner frequency of the source spectrum. Instead, our results may be more consistent with a rupture process in which the length scale of fault zone complexity, rather than event size, controls the high frequency spectral content and radiation pattern (Tsai and Hirth, 2020). In the near-source region, we begin to observe significant distortion of the P-wave radiation pattern only at frequencies above ~ 15 Hz. Assuming a nominal P-wave speed of 6 km/s, this corresponds to a length scale of 300 m. Detailed structural (Kolawole et al., 2019) and seismological (Skoumal et al., 2019) constraints suggest significant geometric complexity in the fault networks of Oklahoma at this length scale, though a detailed analysis of this type for our study region is beyond our present scope.

Understanding the physical factors driving changes in the radiation pattern as a function of frequency has important implications for seismic hazard analysis. The empirical ground motion prediction equations (GMPEs) employed in many hazard applications often do not explicitly account for radiation pattern effects (Bozorgnia et al., 2014; Gregor et al., 2014), though some do adjust for rupture directivity at long periods (Somerville et al., 1997). Kotha et al. (2019) analyzed the residuals from ground motion prediction equations for earthquakes in Japan and their relation to radiation pattern effects, though by necessity these results are based in large part upon recordings at larger station distances than considered in this study, where scattering effects are more pronounced. Our major contribution here is in the measurement of radiation patterns in the near-source region, where observations to date have been more limited. In this regime, we show that the double-couple term dominates the near-field P-wave radiation patterns of small earthquakes within the frequency bandwidth of interest to structural design (< 10 Hz). However, these findings may not generalize to peak ground motions, which come from shear wave shaking over longer time windows. Moreover, while we do not observe a strong dependence on event size within our dataset, one should be cautious about extrapolating our results to larger magnitudes. Near-source observations of large earthquakes are thankfully rare, but more data will be needed to confirm the implications of our findings for hazards.

References

Aki, K., & Chouet, B. (1975). Origin of coda waves: Source, attenuation, and scattering effects. *Journal of Geophysical Research (1896-1977)*, *80*(23), 3322–3342. https://doi.org/10.1029/JB080i023p03322Balakina, L. M., Savarensky, E. F., & Vvedenskaya, A. V. (1961). On determination of earthquake mechanism. *Physics and Chemistry of the Earth*, *4*, 211–238. https://doi.org/10.1016/0079-1946(61)90006-4Ben-Zion, Y., & Ampuero, J.-P. (2009). Seismic radiation from regions sustaining material damage. *Geophysical Journal International*, *178*(3), 1351–1356. https://doi.org/10.1111/j.1365-246X.2009.04285.xBezanson, J., Edelman, A., Karpinski, S., & Shah, V. B. (2017). Julia: A Fresh Approach to Numerical Computing. *SIAM Review*, *59*(1), 65–98. https://doi.org/10.1137/141000671Bozorgnia, Y., Abrahamson, N. A., Atik, L. A., Ancheta, T. D., Atkinson, G. M., Baker, J. W., et al. (2014). NGA-West2 Research Project. *Earthquake Spectra*, *30*(3), 973–987. https://doi.org/10.1193/072113EQS209MBurridge, R., & Knopoff, L. (1964). Body force equivalents for seismic dislocations. *Bulletin of the Seismological Society of America*, *54*(6A), 1875–1888.Castro, R. R., Franceschina, G., Pacor, F., Bindi, D., & Luzi, L. (2006). Analysis of the Frequency Dependence of the S-Wave Radiation Pattern from Local Earthquakes in Central Italy. *Bulletin of the Seismological Society of America*, *96*(2), 415–426. https://doi.org/10.1785/0120050066Chester, F. M., & Chester, J. S. (1998). Ultracataclasite structure and friction processes of the Punchbowl fault, San Andreas system, California. *Tectonophysics*, *295*(1), 199–221. https://doi.org/10.1016/S0040-1951(98)00121-8Cochran, E. S., Wickham-Piotrowski, A., Kemna, K. B., Harrington, R. M., Dougherty, S. L., & Peña Castro, A. F. (2020). Minimal Clustering of Injection-Induced Earthquakes Observed with a Large-n Seismic Array. *Bulletin of the Seismological Society of America*, *110*(5), 2005–2017. https://doi.org/10.1785/0120200101Dougherty, S. L., Cochran, E. S., & Harrington, R. M. (2019). The LArge-n Seismic Survey in Oklahoma (LASSO) Experiment. *Seismological Research Letters*, *90*(5), 2051–2057. https://doi.org/10.1785/0220190094Dunham, E. M., Belanger, D., Cong, L., & Kozdon, J. E. (2011). Earthquake Ruptures with Strongly Rate-Weakening Friction and Off-Fault Plasticity, Part 2: Nonplanar Faults. *Bulletin of the Seismological Society of America*, *101*(5), 2308–2322. https://doi.org/10.1785/0120100076Fang, Z., & Dunham, E. M. (2013). Additional shear resistance from fault roughness and stress levels on geometrically complex faults. *Journal of Geophysical Research: Solid Earth*, *118*(7), 3642–3654. https://doi.org/10.1002/jgrb.50262Faulkner, D. R., Lewis, A. C., & Rutter, E. H. (2003). On the internal structure and mechanics of large strike-slip fault zones: field observations of the

Carboneras fault in southeastern Spain. *Tectonophysics*, *367*(3), 235–251. https://doi.org/10.1016/S0040-1951(03)00134-3Frohlich, C. (1994). Earthquakes with Non—Double-Couple Mechanisms. *Science*, *264*(5160), 804–809. https://doi.org/10.1126/science.264.5160.804Graves, R., & Pitarka, A. (2016). Kinematic Ground-Motion Simulations on Rough Faults Including Effects of 3D Stochastic Velocity Perturbations. *Bulletin of the Seismological Society of America*, *106*(5), 2136–2153. https://doi.org/10.1785/0120160088Gregor, N., Abrahamson, N. A., Atkinson, G. M., Boore, D. M., Bozorgnia, Y., Campbell, K. W., et al. (2014). Comparison of NGA-West2 GMPEs. *Earthquake Spectra*, *30*(3), 1179–1197. https://doi.org/10.1193/070113EQS186MHayashida, Y., Matsumoto, S., Iio, Y., Sakai, S., & Kato, A. (2020). Non-Double-Couple Microearthquakes in the Focal Area of the 2000 Western Tottori Earthquake (M 7.3) via Hyperdense Seismic Observations. *Geophysical Research Letters*, *47*(4), e2019GL084841. https://doi.org/10.1029/2019GL084841Honda, H. (1962). Earthquake Mechanism and Seismic Waves. *Journal of Physics of the Earth*, *10*(2), 1–97. https://doi.org/10.4294/jpe1952.10.2_1Huang, Y., & Ampuero, J.-P. (2011). Pulse-like ruptures induced by low-velocity fault zones. *Journal of Geophysical Research: Solid Earth*, *116*(B12), B12307. https://doi.org/10.1029/2011JB008684Huang, Y., Ampuero, J.-P., & Helmberger, D. V. (2014). Earthquake ruptures modulated by waves in damaged fault zones. *Journal of Geophysical Research: Solid Earth*, *119*(4), 3133–3154. https://doi.org/10.1002/2013JB010724Jones, J. P., Okubo, K., Clements, T., & Denolle, M. A. (2020). SeisIO: A Fast, Efficient Geophysical Data Architecture for the Julia Language. *Seismological Research Letters*, *91*(4), 2368–2377. https://doi.org/10.1785/0220190295Julian, B. R., Miller, A. D., & Foulger, G. R. (1998). Non-double-couple earthquakes 1. Theory. *Reviews of Geophysics*, *36*(4), 525–549. https://doi.org/10.1029/98RG00716Kemna, K. B., Peña Castro, A. F., Harrington, R. M., & Cochran, E. S. (2020). Using a Large-n Seismic Array to Explore the Robustness of Spectral Estimations. *Geophysical Research Letters*, *47*(21), e2020GL089342. https://doi.org/10.1029/2020GL089342Kobayashi, M., Takemura, S., & Yoshimoto, K. (2015). Frequency and distance changes in the apparent P-wave radiation pattern: effects of seismic wave scattering in the crust inferred from dense seismic observations and numerical simulations. *Geophysical Journal International*, *202*(3), 1895–1907. https://doi.org/10.1093/gji/ggv263Kolawole, F., Johnston, C. S., Morgan, C. B., Chang, J. C., Marfurt, K. J., Lockner, D. A., et al. (2019). The susceptibility of Oklahoma's basement to seismic reactivation. *Nature Geoscience*, *12*(10), 839–844. https://doi.org/10.1038/s41561-019-0440-5Kotha, S. R., Cotton, F., & Bindi, D. (2019). Empirical Models of Shear-Wave Radiation Pattern Derived from Large Datasets of Ground-Shaking Observations. *Scientific Reports*, *9*. https://doi.org/10.1038/s41598-018-37524-4Liu, H.-L., & Helmberger, D. V. (1985). The 23:19 aftershock of the 15 October 1979 Imperial Valley earthquake: More evidence for an asperity. *Bulletin of the Seismological Society of America*, *75*(3), 689–708.Ma, X., & Elbanna, A. (2019). Dynamic rupture propagation on fault planes with explicit representation of short branches. *Earth and Planetary Science Letters*, *523*, 115702.

14

https://doi.org/10.1016/j.epsl.2019.07.005Mitchell, T. M., & Faulkner, D. R. (2009). The nature and origin of off-fault damage surrounding strike-slip fault zones with a wide range of displacements: A field study from the Atacama fault system, northern Chile. *Journal of Structural Geology*, *31*(8), 802–816. https://doi.org/10.1016/j.jsg.2009.05.002Nakano, H. (1923). Note on the nature of forces which give rise to the earthquake motions. *Seismol Bull Centr Meteorol Obs, Tokyo*, *1*, 92–120.Oliver, J., & Murphy, L. (1971). WWNSS: Seismology's Global Network of Observing Stations. *Science*, *174*(4006), 254–261. https://doi.org/10.1126/science.174.4006.254Peña Castro, A. F., Dougherty, S. L., Harrington, R. M., & Cochran, E. S. (2019). Delayed Dynamic Triggering of Disposal-Induced Earthquakes Observed by a Dense Array in Northern Oklahoma. *Journal of Geophysical Research: Solid Earth*, *124*(4), 3766–3781. https://doi.org/10.1029/2018JB017150Reid, H. F. (1911). *The elastic-rebound theory of earthquakes* (Vol. 6, 19). Berkeley, CA: University of California Publications, Bulletin of the Department of Geology.Rowe, C. D., Ross, C., Swanson, M. T., Pollock, S., Backeberg, N. R., Barshi, N. A., et al. (2018). Geometric Complexity of Earthquake Rupture Surfaces Preserved in Pseudotachylyte Networks. *Journal of Geophysical Research: Solid Earth*, *123*(9), 7998–8015. https://doi.org/10.1029/2018JB016192Satoh, T. (2002). Empirical Frequency-Dependent Radiation Pattern of the 1998 Miyagiken-Nanbu Earthquake in Japan. *Bulletin of the Seismological Society of America*, *92*(3), 1032–1039. https://doi.org/10.1785/0120010153Savran, W. H., & Olsen, K. B. (2020). Kinematic Rupture Generator Based on 3-D Spontaneous Rupture Simulations Along Geometrically Rough Faults. *Journal of Geophysical Research: Solid Earth*, *125*(10), e2020JB019464. https://doi.org/10.1029/2020JB019464Skoumal, R. J., Kaven, J. O., & Walter, J. I. (2019). Characterizing Seismogenic Fault Structures in Oklahoma Using a Relocated Template-Matched Catalog. *Seismological Research Letters*, *90*(4). https://doi.org/10.1785/0220190045Somerville, P. G., Smith, N. F., Graves, R. W., & Abrahamson, N. A. (1997). Modification of Empirical Strong Ground Motion Attenuation Relations to Include the Amplitude and Duration Effects of Rupture Directivity. *Seismological Research Letters*, *68*(1), 199–222. https://doi.org/10.1785/gssrl.68.1.199Takemura, S., Furumura, T., & Saito, T. (2009). Distortion of the apparent S-wave radiation pattern in the high-frequency wavefield: Tottori-Ken Seibu, Japan, earthquake of 2000. *Geophysical Journal International*, *178*(2), 950–961. https://doi.org/10.1111/j.1365-246X.2009.04210.xTakemura, S., Kobayashi, M., & Yoshimoto, K. (2016). Prediction of maximum P- and S-wave amplitude distributions incorporating frequency- and distance-dependent characteristics of the observed apparent radiation patterns. *Earth, Planets and Space*, *68*(1), 166. https://doi.org/10.1186/s40623-016-0544-8Takenaka, H., Mamada, Y., & Futamure, H. (2003). Near-source effect on radiation pattern of high-frequency S waves: strong SH–SV mixing observed from aftershocks of the 1997 Northwestern Kagoshima, Japan, earthquakes. *Physics of the Earth and Planetary Interiors*, *137*(1), 31–43. https://doi.org/10.1016/S0031-9201(03)00006-2Trugman, D. T., & Dunham, E. M. (2014). A 2D Pseu-

dodynamic Rupture Model Generator for Earthquakes on Geometrically Complex Faults. *Bulletin of the Seismological Society of America*, *104*(1), 95–112. https://doi.org/10.1785/0120130138Trugman, D. T., Ross, Z. E., & Johnson, P. A. (2020). Imaging Stress and Faulting Complexity Through Earthquake Waveform Similarity. *Geophysical Research Letters*, *47*(1), e2019GL085888. https://doi.org/10.1029/2019GL085888Tsai, V. C., & Hirth, G. (2020). Elastic Impact Consequences for High-Frequency Earthquake Ground Motion. *Geophysical Research Letters*, *47*(5), e2019GL086302. https://doi.org/10.1029/2019GL086302Vvedenskaya, A. V. (1956). Determination of displacements' fields for earthquakes by means of the dislocation theory. *Izv. Akad. Nauk SSSR*, *3*(3), 277–284.Wessel, P., Luis, J. F., Uieda, L., Scharroo, R., Wobbe, F., Smith, W. H. F., & Tian, D. (2019). The Generic Mapping Tools Version 6. *Geochemistry, Geophysics, Geosystems*, *20*(11), 5556–5564. https://doi.org/10.1029/2019GC008515